

A surviving disk from a galaxy collision at $z = 0.4$

Y. Yang¹, F. Hammer¹, H. Flores¹, M. Puech^{2,1}, and M. Rodrigues¹

¹ GEPI, Observatoire de Paris, CNRS, Université Paris Diderot; 5 Place Jules Janssen, Meudon, France

² ESO, Karl-Schwarzschild-Strasse 2, D-85748 Garching bei München, Germany

Received ; accepted

ABSTRACT

Context. Spiral galaxies dominate the local galaxy population. Disks are known to be fragile with respect to collisions. Thus it is worthwhile to probe under which conditions a disk can possibly survive such interactions.

Aims. We present a detailed morpho-kinematics study of a massive galaxy with two nuclei, J033210.76–274234.6, at $z = 0.4$.

Methods. The morphological analysis reveals that the object consists of two bulges and a massive disk, as well as a faint blue ring. Combining the kinematics with morphology we propose a near-center collision model to interpret the object.

Results. We find that the massive disk is likely to have survived the collision of galaxies with an initial mass ratio of $\sim 4 : 1$. The N-body/Smoothed Particle Hydrodynamics (SPH) simulations show that the collision possibly is a single-shot polar collision with a very small pericentric distance of ~ 1 kpc, and that the remnant of the main galaxy will be dominated by a disk. The results support the disk survival hypothesis.

Conclusions. The survival of the disk is related to the polar collision with an extremely small pericentric distance. With the help of N-body/SPH simulations we find the probability of disk survival is quite large regardless whether the two galaxies merge or not.

Key words. Galaxies: formation – Galaxies: evolution – Galaxies: kinematics and dynamics – Galaxies: interactions

1. Introduction

In the local universe, most of the intermediate-mass galaxies are spiral galaxies (Nakamura et al., 2004) which have experienced a violent merging stage over the last 8 Gyrs (Le Fèvre et al., 2000; Bundy et al., 2004; Rawat et al., 2008). How the local spirals have been formed is still a matter of debate. Hammer et al. (2005) propose a scenario of “disk-rebuilding” based on the remarkable coincidence of the evolution of the merger rate, morphology and fraction of actively star-forming galaxies. In such a scenario, a significant fraction of galaxies have experienced their last major merger during the last 8 Gyrs, then, by accretion of gas and debris, the disks were formed around the merger remnants.

As a prediction of hierarchical models of structure formation (White & Rees, 1978), galaxy-galaxy mergers or interactions have been an essential recipe to interpret the formation and evolution of galaxies (Barnes & Hernquist, 1992; Springel, 2000). Earlier numerical simulations predicted that the remnants of major mergers of disk galaxies (with mass ratio smaller than $\sim 4 : 1$) are likely to be elliptical galaxies (e.g., Barnes, 1988; Barnes & Hernquist, 1992; Hernquist, 1992), implying that the disks of the progenitors are easily destroyed in major mergers. The simulations by Barnes (2002) suggest that gas disks may be rebuilt after major mergers from the orbital angular momentum. Similar results are shown by recent simulations of gas-rich encounters (Springel & Hernquist, 2005; Robertson et al., 2006; Hopkins et al., 2008). While minor mergers are less violent than major ones, the effect of minor mergers in re-shaping progenitors is significant, even with large mass ratios of 10:1 (Toth & Ostriker, 1992). By the accretion of satellite galaxies, a thin disk will become thicker due to the dynamical heating by the satellite in-fall. Although the disks of spiral galaxies may survive minor mergers, their properties, such as the shape, the

star-formation, the bulge-to-disk ratio, are evolving towards the early type spirals (Walker et al., 1996).

One interesting galaxy interaction is head-on collision which may cause the formation of the ring in disk galaxies, so called “collisional” ring galaxies (Lynds & Toomre, 1976). In this case, the satellite galaxy impacts close to the center of the host galaxy, and passes through the disk. Then a ring will be formed and propagate in the disk outwards due to the density wave. Simulations show that in most of the collisional ring galaxies, disks are severely affected (Appleton & Struck-Marcell, 1996; Athanassoula et al., 1997). Therefore it is worthwhile to explore whether a disk will survive the collision, and under what conditions, such as mass ratio and orbital parameters.

We present a morphology and kinematics study of J033210.76–274234.6 which is possibly an indication of such a surviving disk. This paper is organized as follows: in Sect. 2 we describe the data we have obtained for the object; in Sect. 3, the analysis of morphology is presented. In Sect. 4, we develop a dynamical model together with N-body/SPH simulations in order to explain the observations. We discuss the results and give our conclusions in Sect. 5. Throughout the paper, we adopt the Concordance cosmological parameters of $H_0 = 70 \text{ km s}^{-1} \text{ Mpc}^{-1}$, $\Omega_M = 0.3$ and $\Omega_\Lambda = 0.7$.

2. Data

The object J033210.76–274234.6 ($z = 0.41686$) is located in the GOODS field (The Great Observatories Origins Deep Survey, Giavalisco et al., 2004). The public data of GOODS are available for the detailed studies of its colors and morphology. We chose the data release 1.0 from *GOODS Cutout Service*¹ and obtained the images in 4 bands: F435W, F606W, F775W, F850LP, namely

Send offprint requests to: yanbin.yang@obspm.fr

¹ <http://archive.stsci.edu/eidol.php>

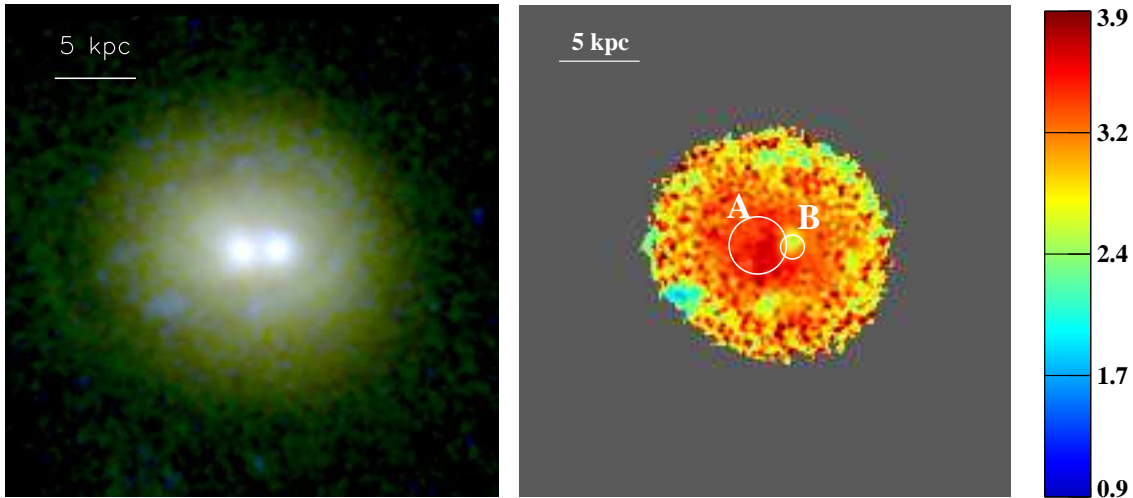


Fig. 1. *Left:* the three-color image composed from the B, V, z bands. The image has a size of 30 kpc. *Right:* B–z color map of the object. The regions with signal-to-noise ratio greater than 3 are shown. The circles A, B indicate core-A and core-B, respectively. The radii of the two circles are equivalent to the effective radii of the two cores. These two panels have identical scale and orientation.

B, V, i, z. The drizzled HST/ACS images have a pixel scale of $0.03''/\text{pixel}$, corresponding to $0.165 \text{ kpc}/\text{pixel}$ at the target redshift. In Table 1 we list the photometric properties of the object.

With the FLAMES-GIRAFFE multi-object integral-field spectrograph at VLT (see Flores et al., 2006), the spatially-resolved kinematics of this object has been recovered by observing the [O II] doublet emission (Yang et al., 2008). The object was early selected into the sample of emission line galaxies (Yang et al., 2008). From the high quality FORS2 spectroscopic observation at VLT (Rodrigues et al., 2008), it is discovered to be a rather quiescent galaxy with weak [O II] emission (at $\sim 2 \text{ \AA}$). Due to the brightness of the object ($V(\text{AB})=19.9$) we are able to recover its kinematics with GIRAFFE at VLT.

3. Analysis

3.1. General properties

In Fig. 1, we show a three-color image and a B–z color map of the object. The color of the three-color image is slightly enhanced for better recognizing the structures. Two bright nuclei can be easily recognized. We have plotted two circles in the B–z color map to indicate the core positions and the sizes at effective radius that are derived from the morphology analysis (see Sect. 3.2). The left core (hereafter core-A), has a color as red as the elliptical galaxies at redshift 0.4 (see Figure 8 of Neichel et al., 2008). The right core (hereafter core-B) is slightly bluer than core-A, and its color is similar to that of an S0 galaxy. In addition, we detect several blue clumps surrounding the object center. Since it resembles a ring, we refer to it as the “blue ring” hereafter. It is detected in B-band which corresponds to U-band at rest frame. This suggests that star formation has been triggered in the ring.

3.2. Morphological analysis

GALFIT (Peng et al., 2002) is used to perform a two-dimensional profile decomposition in order to study the intrinsic luminosity distribution. The technical details about the decomposition have been discussed in Neichel et al. (2008) and Rawat et al. (2007). We chose the Sérsic profile to model each component. The key

Table 1. Properties of the target J033210.76–274234.6.

Photometric properties:						
$M_B(\text{AB})$	$M_J(\text{AB})$	R_{half}^*	$M_{\text{stellar}}^{\text{total}}$	SFR _{IR}	SFR ₂₈₀₀	A_V
		(kpc)	($10^{10} M_{\odot}$)	(M_{\odot}/yr)	(M_{\odot}/yr)	
−21.78	−23.70	4.36	27.5	5.27	3.24	0.2
Morphological decomposition for z-band						
	Magnitude	$R_{\text{eff}}^{\text{a}}$ (kpc)	F_i^{b}	B–z ^c		
core-A	20.03±0.01	1.78±0.02	0.27±0.01	3.53		
core-B	20.85±0.01	0.74±0.01	0.13±0.01	3.15		
Disk	19.14±0.01	5.39±0.01	0.60±0.01	2.94		
	Center ^d	P.A. ^e	Inc. (b/a) ^f	$M_{\text{stellar}}^{\text{g}}$		
	(kpc)	(°)		($10^{10} M_{\odot}$)		
core-A	[0.00, 0.00]	69	0.75	3.57		
core-B	[2.15, −0.10]	65	0.82	7.43		
Disk	[0.67, 0.03]	65	26°	16.5		
Blue Ring	[0.02, 0.12]	−78	52°	—		
Physical scales						
The distance of the two cores		2.15 kpc				
The radius of the blue ring		7.18 kpc				

* The half-light radius. ^a The effective radius of the Sérsic profile. ^b The light fraction of each model component with respect to the total model flux. ^c The B–z color of each component, calculated based on the morphological decomposition. ^d The center of each component, measured with respect to the center of the disk. ^e The position angle of each component. ^f For the disk and the ring we give the inclination in degrees; for the bulges we give the axis ratios. ^g The stellar mass of each component (see Sect. 4 for details).

parameter is the Sérsic index n , which gives the classical bulge profile of the de Vaucouleurs law when $n = 4$, and the exponential disk when $n = 1$.

We first investigated the light profile of z-band. We initially set a model of two Sérsic profiles that are centered at the two nuclei respectively. GALFIT gives a best fit with χ^2/ν of 1.88. The significant residuals imply the existence of an additional component. We then added the third component of Sérsic to the model. We get an optimized solution of $\chi^2/\nu = 1.26$ with $n = 5.67, 4.61, 0.48$ for core-A, core-B and the third component, respectively. The two nuclei are bulges since their n approximate to 4. The

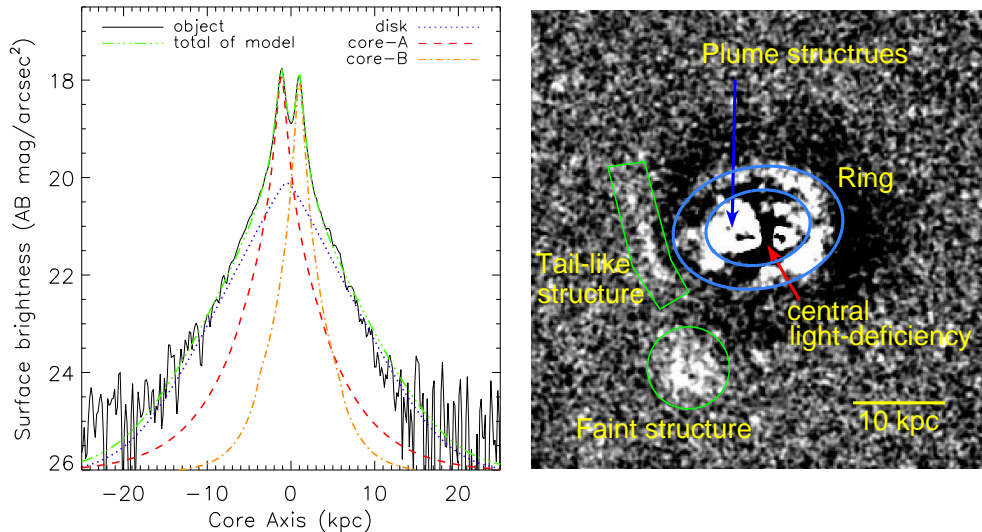


Fig. 2. *Left:* light profile decomposition along the core-axis of z-band. *Right:* the V-band residual image (slightly smoothed) of morphology decomposition. The blue annulus indicates the ring region. The other two green regions indicate the tail-like structure and the faint structure, respectively. The plume structures and the central light-deficiency are marked by arrows as well.

third component resembles the disk shape according to its lower n . We have tried a four-component model which gave no improvement. Alternatively, we have tried to bind the disk center to any of the cores, but no reasonable solutions were found. It is known that the Sérsic index is coupling to the effective radius (Peng et al., 2002; Trujillo et al., 2001). Thus we fixed the index n to the classical values: $n = 4$ for bulges and $n = 1$ for the disk-like component. We obtained a reasonable fit with a χ^2/ν of 1.34. Although χ^2 of the free- n fit is smaller than that of the fixed- n fit, it does not significantly improve the modeling. So we adopt the fixed- n model hereafter. We have performed fixed- n fitting to the other three bands (i.e., B, V, i). The findings are similar to what we get from z-band. As a result, we have successfully recovered the main components of the object, i.e., the two bulges and the large disk centered between the two. The parameters of each component in z-band and the error estimation by GALFIT are listed in Table 1.

The left panel of Fig. 2 illustrates the results of the morphological decomposition. We show the light profile along the core-axis which is defined to be the line across the centers of the two bulges. The profile of each seeing-convolved model component as well as the sum of them are plotted separately in Fig. 2 with different symbols. The light profile at $|r| > 5$ kpc is close to a straight line, which is strongly indicative of the existence and the significance of the disk. The center of the disk is found to be located between the two nuclei (close to core-A), and no significant structures, e.g., arms, are found in the disk. Note that in the residual maps of all the bands, we find several structures (see V-band for example, the right panel in Fig. 2), including a shell-like structure following the blue ring, plume-like structures that are associated with core-A, a tail-like structure and a faint structures. These residuals indicate a recent galactic interaction in the object.

4. Dynamical model

4.1. Analysis

The detection of a ring suggests that an almost central collision took place between two progenitors. The morphological analysis shows a very strong indication that the disk of main progenitor

was relatively little affected by this interaction, as weak perturbations are detected in the residuals. Below, with the help of N-body/SPH (e.g., Monaghan, 1992) simulations, we construct a model for this collision in order to test whether the main progenitor disk may have survived the interaction.

With the spatially-resolved kinematics from GIRAFFE, the slit kinematics from FORS2, and the morphological decomposition, we are able to develop a dynamical model to interpret the interaction occurring in the object. The mass of each component is crucial to construct the model. We have obtained the stellar mass of the system from Puech et al. (2008) and listed it in Table 1. We estimate the stellar mass of each component according to their z-band light fraction (see Table 1), under the assumption that the luminosity in z-band (corresponding to R-band at rest frame) is approximately proportional to the stellar mass.

The panel (a) of Fig. 3 shows a 3D sketch of the object based on the morphological parameters that are derived from the decomposition. The disk is nearly face-on with an inclination of 26° . The two bulges have a projected distance of 2.15 kpc. The blue ring with an inclination of 52° is also shown in the figure. The ring has a radius of 7.18 kpc. The two plumes (Fig. 2) may be the tidal relics of the core collision, because they have a red color similar to core-A which is marginally affected by the global low extinction $A_V = 0.2$ (see Table 1). Moreover, we find that the center of core-B in B-band is slightly shifted from the centers in the other bands by $0.06''$ (~ 0.3 kpc). This shift may account for the asymmetric color distribution of core-B (see B-z map Fig. 1).

What are the progenitors? The detection of the giant disk is robust. This disk does not seem to be severely affected by the collision. We refer to the galaxy associated with this disk as the main galaxy. We have noticed that the B-z color of the disk is 2.94 which is in agreement with the color of S0 galaxies at this redshift (see Figure 8 of Neichel et al., 2008). From its location, brightness and color, core-A is likely to be the bulge of the main galaxy. If we take core-B as the bulge of the main galaxy, resulting in a bulge-to-total light ratio of $B/T \sim 0.17$, then we would expect a bluer disk such as Sbc type galaxies. The inclination of the blue ring is quite high compared to that of the detected disk. This suggests that the blue ring is probably not lying in

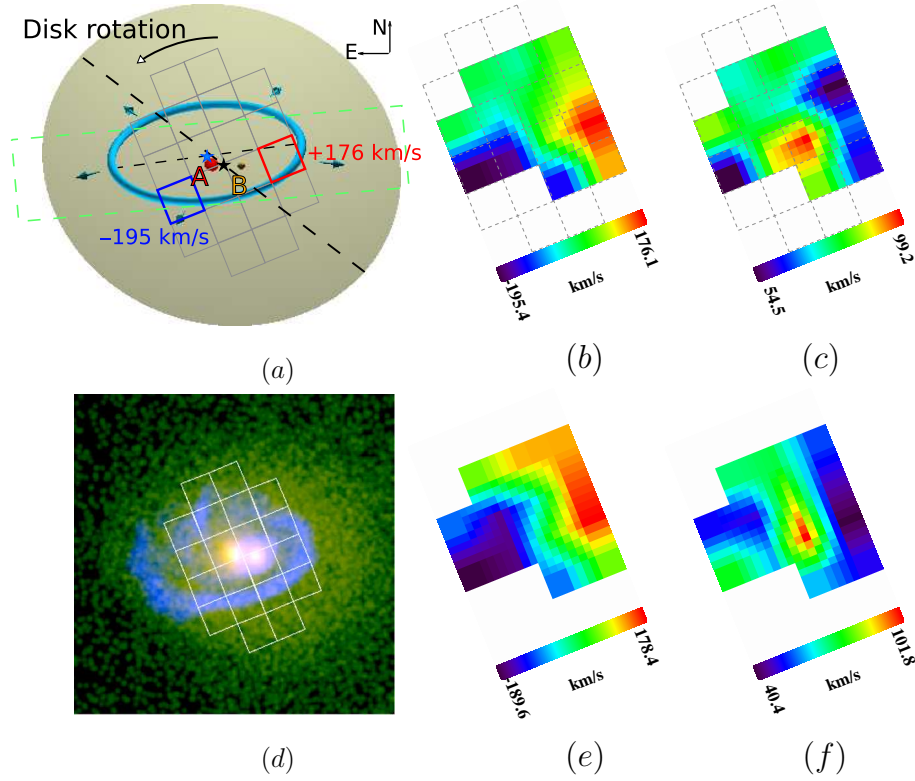


Fig. 3. Panel (a), a 3D sketch of our target based on the morphological decomposition. The disk is represented by a gray plane. The two bulges are indicated by different colors, red for core-A and orange for core-B. The blue ring is shown as well in blue. Two black dashed lines indicate the major axes of the ring and the disk, respectively. The black star between the two bulges represents the center of the disk. The blue star above the core-A indicates the center of the ring. The rotated grid in gray lines indicates the GIRAFFE IFU elements (see panels (b) and (c)). The red and the blue boxes highlight the maximal and the minimal velocities observed by GIRAFFE IFU. The green dashed box indicates the position and the coverage of the FORS2 slit. Panels (b) and (c), the spatially-resolved kinematics, i.e., the velocity field and the velocity dispersion, respectively. The dashed-line grids indicate the spatial resolution elements of IFU. The kinematics maps have been rotated to be aligned with the object orientation. Panel (d) shows the simulated image which is constructed by the projected star density (in yellow-green) with the gas superposed in blue color. Panels (e) and (f) show the simulated gas kinematics: VF- and σ -maps (see Sect. 4 for more details).

the plane of the disk. It implies that another disk existed before the collision, and this disk had been disrupted during the collision and formed the ring. From the morphology decomposition, we have estimated the bulge mass of the two progenitors: for the main galaxy, the bulge takes 27% of the total mass of the system, and for the intruder, the bulge takes 13%. It is difficult to estimate the exact mass ratios of the progenitors, since the intruder’s disk had been disrupted. However, we can estimate the limits. We have observed the star-forming activities, i.e., the blue ring which suggests a significant fraction of gas preexisted in the intruder disk. First, let us assume the intruder is an Sa galaxy with B/T of 0.3 which is a typical value for Sa galaxies. With this assumption, we arrive at a mass ratio of $\sim 1:1$ between the progenitors. This seems not the case that we have observed. Otherwise we would have seen two rings with similar strength. Thus, the intruder could be an S0 galaxy with B/T ranging from 0.5 to 0.8. We assume a mean B/T value of 0.65 for the intruder, which gives a mass ratio of 4:1 for the progenitors. Even if we take B/T = 0.8, the mass ratio only increases to 5:1 which could be the upper limit of mass ratio. We adopt a mass ratio of 4:1 in the following discussion, resembling a major merger as usually mentioned.

We have obtained FORS2 slit observations of the object from Rodrigues et al. (2008), see Fig. 3 for the slit coverage. Using the absorption lines Ca II H, K, we are able to recover a velocity

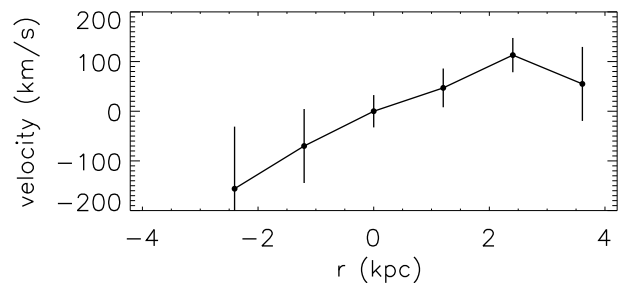


Fig. 4. The velocity curve of the object, which is derived from the FORS2 slit observation. The coverage of slit is shown in the panel (a) of Fig. 3 in a green dashed-line box.

curve covering the central 7.2 kpc region (see Fig. 4), which suggests a disk dominated by rotation. With the maximal ΔV of 269 km s^{-1} , the rotation velocity is estimated to be 360 km s^{-1} after correcting for disk inclination. With the mass ratio of 4:1, we can derive the stellar mass of the main galaxy to be $2.2 \times 10^{11} M_{\odot}$ (80% of the total). We find that this galaxy is well in agreement with the stellar mass Tully-Fisher relation by Puech et al. (2007) and with the R_d - V_{flat} relation by Hammer et al. (2007).

The right panel of Fig. 3 shows the GIRAFFE 2D velocity field (VF) and velocity dispersion (σ) map. Since the maps are de-

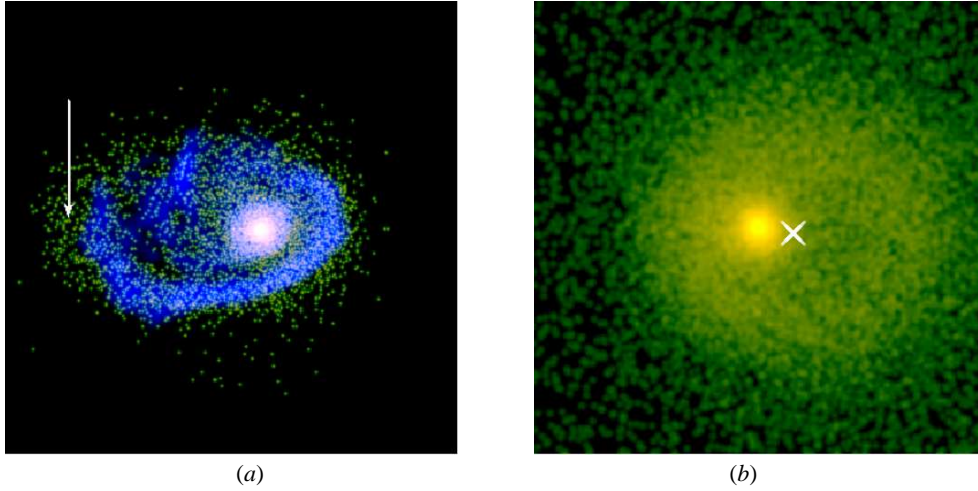


Fig. 5. Panel (a), the simulated image for the intruder only, with gas superposed in blue color. The arrow indicates the star distribution which is possibly corresponding to the observed tail-like structure. Panel (b), the simulated image for the main galaxy only. A weak but broad ring can be recognized. Due to the superposition of the bulge, the left part of the ring shape is hidden. The cross indicates the center of the disk. See Sect. 4.2 for more details.

rived from the [O II] emission, the kinematics tracks the large-scale motion of the gas. The dynamical axis, which is defined as the line connecting the minimum and maximal velocity, is misaligned with the major axis of the ring. This suggests that the motion of gas is not a simple rotation pattern, and that another motion is superposed on it. The velocity gradient follows the ring. The above facts are easily explained by the superposition of a disk rotation and an expanding velocity field related to the ring. We estimate the expanding velocity of the ring to be $180 \pm 70 \text{ km s}^{-1}$ by taking into account the geometric projection and several GIRAFFE measurements around the ring. This suggests the elapsed time after the impact to be 39 Myrs by taking the ring radius of 7.18 kpc.

4.2. N-body/SPH simulation

With the geometrical parameters and mass ratios derived above, we have constructed N-body/SPH simulations to demonstrate the formation of the blue ring and to test the disk survival hypothesis. We used the N-body/SPH software called “ZENO” which is developed by Barnes² (e.g., Barnes & Hernquist, 1992). Galaxy models are created following Barnes (1988, 2002). In the “ZENO”, we have $G = 1$. The mass ratio between two galaxies is set to be 4:1. Using the same fraction of halo and baryonic matter as in Barnes (2002), the total mass of the system was set to 3.25 mass units. With the stellar mass of the system, $2.75 \times 10^{11} M_{\odot}$, we get the mass unit of simulation as $4.4 \times 10^{11} M_{\odot}$. Then we chose the length scale 38.6 kpc, resulting in the velocity unit of 221 km s^{-1} and the time unit of 176 Myrs. For the main progenitor, we adopted $B/T=0.34$, scale length of 5.27 kpc and scale height of 2.5 kpc; while for the intruder, $B/T=0.65$, scale length of 3.0 kpc, and scale height of 0.5 kpc. We assume 5% of gas distributed in the intruder disk, and no gas in the main galaxy. The gas has the same properties as in Barnes (2002), and the SPH calculation follows the isothermal equation of state. Our simulations include $N_{\text{halo}} + N_{\text{star}} + N_{\text{gas}} = 45000 + 44856 + 7560 = 97416$ particles. The gas fraction in our system is very low. Therefore, we chose a small mass resolution for SPH calculation in order to have a reasonable number of particles to trace the gas motion.

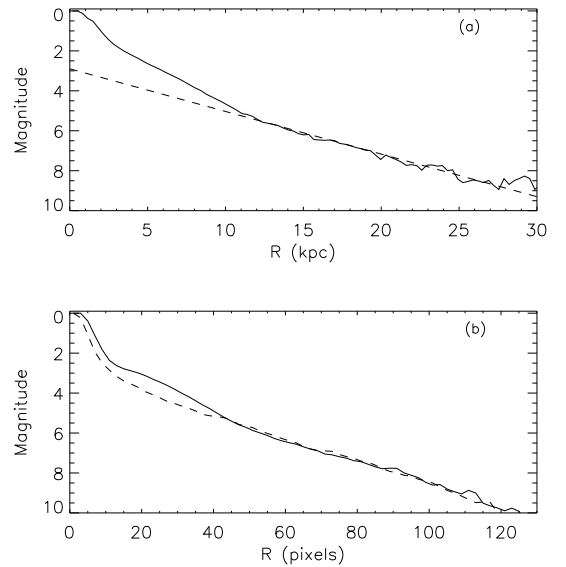


Fig. 6. Panel (a), the observed radial profile (solid line). The dashed line indicates the slope of the thin-disk component. At the radii from 5 to 10 kpc, we clearly have a thick-disk component which corresponds to the ring that has been formed in the disk of main galaxy. Panel (b), the radial profile derived from the simulation. Clearly we have a thin- and a thick-disk component. The appearance of the thick-disk component is related to the formation of the ring. For comparison, the radial profile of the main progenitor is plotted as dashed line.

We designed a polar collision that follows a parabolic orbit with pericentric separation of ~ 0.76 kpc. The fine-tuning of orbital parameters³ is necessary to closely match the morphology and the gas kinematics.

³ In the ZENO system, the exact parameters we adopted for the current model are, at $t=-0.12$ from the first passage, $\text{deltar}=0, 0, 0.5$, $\text{deltav}=-0.56, 0.38, -3.5$, the orientation of intruder $\text{thetax}=35$, $\text{thetay}=-25$, $\text{thetaz}=0$ and the orientation of the main $\text{thetax}=18$, $\text{thetay}=18$, $\text{thetaz}=55$

² <http://www.ifa.hawaii.edu/~barnes/software.html>

This simulation matches both the morphology and the kinematics that we observed, as well as some detailed features. Below, we list those particular features that are matched by the simulation. The strongest constraints are the ACS morphology and the GIRAFFE kinematics.

1. In Fig. 3(d), we show a simulated image⁴ that is constructed by the projected star density with the gas superposed in blue color. The observed blue ring is defined by rest-frame U-band clumps which indicate the star-burst regions. Thus the blue ring basically traces the gas. In the simulation, a gas ring begins to form after the first passage, and evolves 35 Myrs to match the observation. Note that the gas ring in the simulation has a slightly larger size than the observed blue ring in order to match the GIRAFFE kinematics. On the other hand, this is expected since the stellar evolution is found to be behind the expanding density wave (Appleton & Struck-Marcell, 1996).
2. The kinematics of the object from GIRAFFE is derived from [O II] doublet emission that is coming from the ionized gas. In Fig. 3(e, f), we show kinematics of gas from the simulation. Geometrically and quantitatively, the simulated gas kinematics is in good agreement with the observation, i.e., the dynamical axis of the velocity field and the peak of the velocity dispersion.

Furthermore, the simulation shows consistencies in several details.

3. In Fig. 1, we may notice the slight distortion of the morphology at the left part of the ring, close to the edge of the ring. This distortion can be seen also in the B-z color-map. In the simulated image, we find the same feature. The distortion is due to the superposition of the two galaxies.
4. Both the three-color image of Fig. 1 and the residual image of Fig. 2 show a tail-like feature. From the simulation we find that it is likely to be the tidal tail created by the collision. In Fig. 5(a), we compare the gas and the stellar component for the intruder galaxy. We notice that the stars move further than the gas, marked by the an arrow in the figure. Their relative position resembles the blue ring and the tail-like structure in the observation. The simulation does not show an exact tail structure. Nevertheless, the star dynamics has been demonstrated reasonably well.
5. Our target J033210.76–274234.6 is a strong galactic collision. We have estimated that the mass ratio of progenitors is not larger than 5 : 1, and adopted 4:1 in modeling. The intruder penetrated the center of the main galaxy. A ring in the main galaxy is expected to be observed, as we have seen in the simulation (see Fig. 5b). Although we cannot see the ring directly, we have found two robust observational evidences, enlightened by the simulation, to prove its existence. In Fig. 6, we compared the observed radial profile with the simulated one. Both of them exhibit two disk components: a thick disk and a more extended thin disk. Note that for the observation, the thin disk is only detected in the radial profile. Hence, from the simulation, we may conclude that the thick-disk component is caused by the formation of the ring. This leads to the realization that the disk we have seen in the three-color figure is actually the ring that has formed in the

⁴ 1) All the simulated images in this paper are created by the projected density of particles directly. Thus the gas component is emphasized by a factor of 50 times due to the large number of gas particles. 2) All the simulated images, except Fig. 8, have been scaled to the same physical size as Fig. 1.

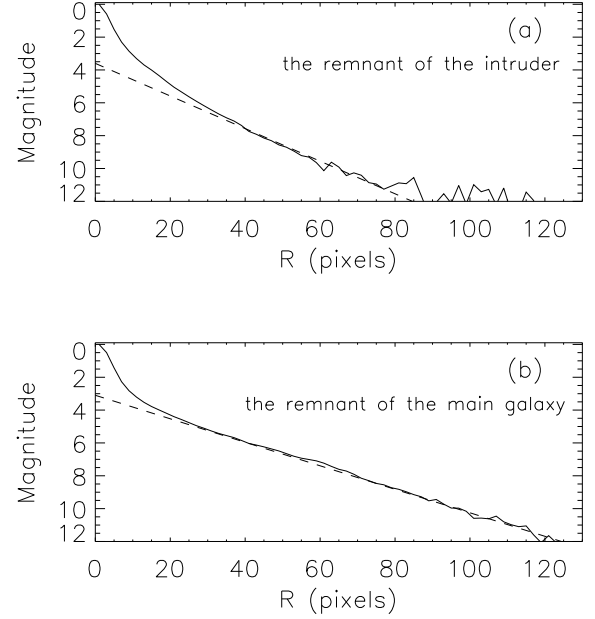


Fig. 7. The radial profiles of the remnants in the unbound case, panel (a) for the remnant of the intruder, (b) for the remnant of the main galaxy. The dashed lines in both figures indicate the disk components. Clearly, the remnant of the main progenitor is dominated by the disk.

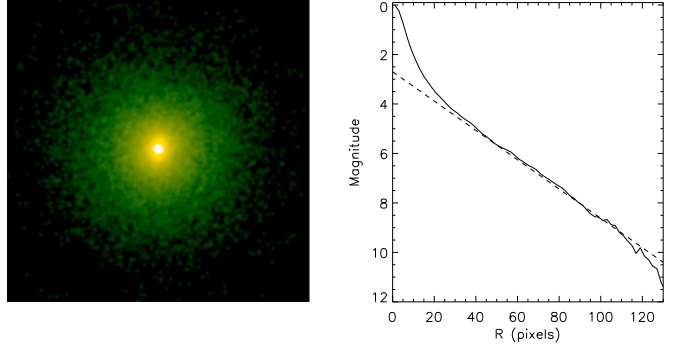


Fig. 8. *Left:* The face-on view of the merger remnants. The image has a size of 103 kpc. *Right:* the radial profile of the merger remnant. The disk component is indicated by a dashed line.

main galaxy. The second evidence is from the residual image (see Fig. 2) where we have marked a light-deficiency region in the central part. It is naturally explained when a disk with a ring is fitted and subtracted by a disk profile. Therefore, the ring in the main galaxy has been observed. However, due to the superposition of the two bright bulges and the broadness of the ring, the shape of the ring is hidden. The broadness of the ring is linked to the thickness of the main disk, which has been investigated and proved by our simulations.

6. In the previous section, we mentioned that the center of core-B in B-band is slightly shifted from other bands, resulting the asymmetric color distribution of core-B (see Fig. 1). In the simulation, we have observed that, after the first passage, part of the perturbed gas is falling back to the center of the intruder. The falling gas may cause the star-forming activi-

ties which could explain the color shift of core-B. Note that, from the simulation, we find that the maximum velocity in the VF map is also caused by the infalling gas.

7. The morphology decomposition reveals that the bulge of the main progenitor, core-A, has been shifted from the center of the disk. This is also confirmed by the simulation. In Fig. 5b, the bulge of the main galaxy is clearly shifted with respect to the center of the disk. The movement of the central bulge is due to the very close core interaction.
8. From the FORS2 slit spectrum, we have a constraint for the collision speed. We measured the velocity difference between the [O II] emission and Ca II H, K absorption lines, finding $210 \pm 50 \text{ km s}^{-1}$. Note that by measuring the absorption lines we are actually measuring the mean velocity of the two bright bulges when considering seeing effects. Using the simulation, we mimicked the slit observation and measured the mean velocity of star particles and of gas particles, respectively. We find a velocity difference of $270 \pm 60 \text{ km s}^{-1}$ which is consistent with the value from the observation.

To know if the disk of progenitors will be destroyed by the collision, we have explored the remnants by simulations. In our simulation, the collision speed at the first passage is $\sim 1200 \text{ km s}^{-1}$ and the two objects are departing at the speed of $\sim 500 \text{ km s}^{-1}$ at the observing time. They are not a gravitationally bound system. We keep the simulation running another 2 Gyrs. The remnants of the both galaxies show a disk component. Especially, the remnant of the main galaxy is still dominated by disk. In Fig. 7, we plotted the radial profile of the two remnants. Furthermore, we have run a simulation with lower collision speed, in order to investigate the remnant in case that the two galaxies can be merged. We find that the merger remnant still has a significant disk component at 3.5 Gyrs after the first passage, see Fig. 8.

5. Discussion & Conclusion

Morpho-kinematics analysis reveals that J033210.76–274234.6 is dominated by a massive disk. The spatially-resolved kinematics appears to be the superposition of the rotation and the expanding velocity field from the blue ring. We propose a near-center collision model which explains all the observations. Consequently, we conclude that the disk of the main galaxy has survived the galaxy collision. Followed by the N-body/SPH simulations, we have successfully reproduced the ACS morphology and the GIRAFFE kinematics, as well as some details. With the help of the N-body/SPH simulations, we have explored the remnants of the collision. We find that this is a rare polar collision with a very small ($\sim 1 \text{ kpc}$) pericentric separation, and that regardless of whether the two galaxies merge or not, the remnant of the main galaxy is dominated by disk component. The results support the disk survival hypothesis. The survival of the main disk is related to the exceptional collision with the extremely small pericentric distance and the polar orbit.

Acknowledgements. We would like to thank the referee for the constructive comments. We would like to thank Isaura Fuentes-Carrera, Benoit Neichel and Sebastien Peirani for the helpful discussions. We are grateful to Albrecht Rüdiger for helping us in the writing of the paper. Especially, we would like to thank Joshua E. Barnes for his help on the simulations.

References

Appleton, P. N., & Struck-Marcell, C. 1996, *Fundamentals of Cosmic Physics*, 16, 111

- Athanassoula, E., Puerari, I., & Bosma, A. 1997, *MNRAS*, 286, 284
 Barnes, J. E. 1988, *ApJ*, 331, 699
 Barnes, J. E., & Hernquist, L. 1992, *ARA&A*, 30, 705
 Barnes, J. E. 2002, *MNRAS*, 333, 481
 Bundy, K., Fukugita, M., Ellis, R. S., Kodama, T., & Conselice, C. J. 2004, *ApJ*, 601, L123
 Flores, H., Hammer, F., Puech, M., Amram, P., & Balkowski, C. 2006, *A&A*, 455, 107
 Gialvalisco, M., et al. 2004, *ApJ*, 600, L93
 Hammer, F., Flores, H., Elbaz, D., Zheng, X. Z., Liang, Y. C., & Cesarsky, C. 2005, *A&A*, 430, 115
 Hammer, F., Puech, M., Chemin, L., Flores, H., & Lehnert, M. D. 2007, *ApJ*, 662, 322
 Hernquist, L. 1992, *ApJ*, 400, 460
 Hopkins, P. F., Cox, T. J., Younger, J. D., & Hernquist, L. 2008, *ArXiv e-prints*, 806, arXiv:0806.1739
 Le Fèvre, O., et al. 2000, *MNRAS*, 311, 565
 Lynds, R., & Toomre, A. 1976, *ApJ*, 209, 382
 Monaghan, J. J. 1992, *ARA&A*, 30, 543
 Nakamura, O., Fukugita, M., Brinkmann, J., & Schneider, D. P. 2004, *AJ*, 127, 2511
 Neichel, B., et al. 2008, *A&A*, 484, 159
 Peng, C. Y., Ho, L. C., Impey, C. D., & Rix, H.-W. 2002, *AJ*, 124, 266
 Puech, M., Hammer, F., Lehnert, M. D., & Flores, H. 2007, *A&A*, 466, 83
 Puech, M., et al. 2008, *A&A*, 484, 173
 Rodrigues et al., 2008, *A&A in press*, (astro-ph/0810.0272)
 Rawat, A., Kembhavi, A. K., Hammer, F., Flores, H., & Barway, S. 2007, *A&A*, 469, 483
 Rawat, A., Hammer, F., Kembhavi, A. K., & Flores, H. 2008, *ApJ*, 681, 1089
 Robertson, B., Bullock, J. S., Cox, T. J., Di Matteo, T., Hernquist, L., Springel, V., & Yoshida, N. 2006, *ApJ*, 645, 986
 Springel, V. 2000, *MNRAS*, 312, 859
 Springel, V., & Hernquist, L. 2005, *ApJ*, 622, L9
 Trujillo, I., Graham, A. W., & Caon, N. 2001, *MNRAS*, 326, 869
 Toth, G., & Ostriker, J. P. 1992, *ApJ*, 389, 5
 Walker, I. R., Mihos, J. C., & Hernquist, L. 1996, *ApJ*, 460, 121
 White, S. D. M., & Rees, M. J. 1978, *MNRAS*, 183, 341
 Yang, Y., et al. 2008, *A&A*, 477, 789

List of Objects

- ‘J033210.76–274234.6’ on page 1
 ‘J033210.76–274234.6’ on page 1
 ‘J033210.76–274234.6’ on page 2
 ‘J033210.76–274234.6’ on page 6
 ‘J033210.76–274234.6’ on page 7